THE JOURNAL OF PHYSICAL CHEMISTRY C

pubs.acs.org/JPCC Article

Maximizing Amplified Energy Transfer: Tuning Particle Size and Dye Loading in Conjugated Polymer Nanoparticles

Lisa S. Graves,[†] Matthew J. Goodwin,[†] Isabelle N. Maricar, Jaclyn A. Rebstock, and Elizabeth J. Harbron*

Cite This: *J. Phys. Chem. C* 2020, 124, 26474−26485 Read Online

ABSTRACT: We investigate amplified energy transfer in conjugated polymer nanoparticles (CPNs or Pdots) by studying both fluorescence quenching of CPN donors and the sensitization of reactive dye acceptors. By delivering excitation energy to dye dopants via a combination of Förster energy transfer and exciton diffusion, CPNs act as powerful light-harvesting antennae. This phenomenon—amplified energy transfer—is used to sensitize dye dopants, producing a higher concentration of the dye's excited state than would be observed upon direct excitation. Here, we study CPN sensitization of a low-efficiency photochemical reaction to determine the CPN size and dye loading that yield optimized outputs in the form of energy transfer efficiency, the antenna effect (AE), and reaction duration. Our model system is the cycloreversion reaction of a diarylethene (DAE) photochrome as the dye dopant and CPNs of the conjugated polymer poly[(9,9-dioctylfluorenyl-2,7-diyl)-*co*-1,4-benzo-{2,1′-3}-thiadiazole] as the sensitizer. In their visible-absorbing form, DAE dyes are localized on the particle surface and are effective fluorescence quenchers of 15, 20, and 26 nm diameter CPNs. Quenching is most efficient for the smallest particles, and high dye loadings are necessary to offset reduced efficiency as CPN size increases. Our photokinetic studies of DAE acceptors demonstrate the crucial importance of dye loading: both energy transfer efficiency and the AE show abrupt declines when the dye concentration is increased beyond a critical threshold. We find that CPNs with a 15 nm diameter exhibit the most efficient energy transfer (99−100%) and the largest AE (32) of the CPNs studied. For CPNs of all sizes and dye loadings, a photoselection phenomenon reveals that the energy-transfer-accepting ability of the DAE dyes varies tremendously within the dye ensemble. These findings are used to develop design recommendations for CPN sensitizers.

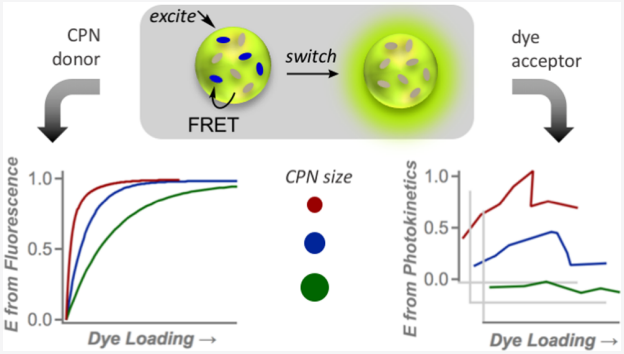

INTRODUCTION

The ideal chemical reaction occurs cleanly, in a timely fashion, and with high conversion to products. Photochemical reactions, in which light serves as a reagent, can meet these criteria with the added benefit that light can be delivered to the reactant with spatiotemporal control. While many photochemical reactions are fast and high-yielding, some are not because their low quantum efficiencies limit reaction rates and conversion to products. This limitation can be overcome by increasing the irradiation intensity and/or duration to achieve the needed product yield. However, prolonged irradiation can have deleterious consequences ranging from chromophore photobleaching to the formation of unwanted side products.

Photosensitization is an alternative approach to low-efficiency photochemical reactions that involves excitation of a sensitizing moiety to generate the reactant's excited state. Fluorescence resonance energy transfer (FRET) is one mechanism by which sensitization can occur. If the donor−acceptor pair undergoes efficient FRET, sensitization can produce a higher concentration of the desired excited state of the acceptor than would be obtained by direct excitation. Sensitization of photochemical reactions by energy transfer has been used to access specific excited states and/or enhance reactivity in photoremovable protecting groups[1] and photochromic moieties,[2,3] among others. Multichromophoric sensitizers can absorb more light than their small-molecule counterparts and have been useful in applications such as artificial photosynthetic systems.[4] We seek to enhance the reaction rates and product yields of low-efficiency photochemical reactions by employing conjugated polymer nanoparticles (CPNs or Pdots) as multichromophoric sensitizers for photoreactive dyes. Here, we present studies of FRET

Received: October 6, 2020
Revised: November 2, 2020
Published: November 19, 2020

https://dx.doi.org/10.1021/acs.jpcc.0c09084
J. Phys. Chem. C 2020, 124, 26474−26485

sensitization of a low-efficiency reaction from both donor and acceptor perspectives. We determine the nanoparticle size that yields the most effective sensitization and discover an unexpected threshold effect that determines the optimal dye loading.

CPNs are small, spherical particles that are stably suspended in aqueous media and exhibit bright, photostable fluorescence. Their emission properties have recently garnered intense attention for imaging and theranostic applications.[5−11] The multichromophoric CPNs are exceptional light absorbers, with extinction coefficients in the range of 10^7-10^8 M^{-1} cm^{-1}.[12] They are outstanding FRET donors because of their ability to harvest light and deliver it efficiently to dye dopants.[13] The efficiency with which an excited CPN chromophore generates an excited dye involves both Förster energy transfer and intrinsic exciton diffusion processes within the CPN that relay donor excitation to acceptor dyes. These processes are highly convolved, and it is not always possible to separate their effects in experimental data. In the present work, we will use the terms "FRET" or "energy transfer" to refer to the convolution of processes that delivers excitons to acceptors and "Förster transfer" and "exciton diffusion" to refer to the individual processes. The interplay between Förster transfer and exciton diffusion has been explored extensively in CPNs doped with fluorescent dyes that are not photochemically reactive.[14−17] For example, Jiang and McNeill have demonstrated that CPN fluorescence quenching that involves both Förster transfer and exciton diffusion can be 2 to more than 4 times more efficient than Förster transfer alone.[13] Energy transfer from CPN donors is referred to as "amplified FRET" for this reason.[13,18] Highly efficient CPN-to-dye FRET has been used to amplify a fluorescence signal for sensing applications, which have been reviewed.[19,20] We[21−23] and others[24−33] have also used FRET from CPNs to nonfluorescent photochromic dyes to modulate the CPNs' fluorescence. While some of these phenomena could also be explained by other fluorescence quenching mechanisms, Algar recently concluded that FRET is the dominant quenching mechanism in a detailed study of dye-doped CPNs.[17]

Applications of dye-doped CPNs[34] have largely been focused on the fluorescence output: dyes are used to shift the CPNs' emission wavelength to lower energy, act as a receptor for fluorescence sensing applications, or modulate fluorescence intensity.[5,20] In our recent study of fluorescence intensity modulation in dye-doped CPNs, we determined that FRET sensitization of a low-quantum-yield photochromic dye could drive the dye's slow, inefficient reaction nearly all the way to completion in just seconds.[35] Our findings are emblematic of an emerging body of literature that focuses on what sensitization by CPNs can do for dyes rather than what dyes can do for CPNs in the form of emission tuning. For example, several groups have demonstrated that CPN-sensitized dyes can produce singlet oxygen for photodynamic therapy applications.[36−40] Applications such as this use the CPNs as amplifiers to generate a higher concentration of the dye's excited state than would be possible upon direct excitation of the dye with comparable light intensity. The dye's excited state is then deactivated by a subsequent photochemical reaction or photophysical process that would occur only rarely without the sensitization.

The use of CPNs as sensitizers for inefficient photochemical reactions or photophysical processes requires high CPN-to-dye FRET efficiency. The groups of McNeill[15] and Redmond[16] have investigated FRET efficiency in dye-doped CPNs as a function of nanoparticle size. For CPNs with dyes randomly distributed throughout the particles, energy transfer efficiency increases as particle radius increases from 5 to 20 nm before leveling off around 30 nm.[15,16] Most of these results come from simulation rather than from the experiment and involve dyes with high extinction coefficients that are excellent FRET acceptors. Additionally, the relationship between FRET efficiency and CPN size has not been investigated for CPNs in which the dye dopants are located only on the particle surface or for those in which the dyes are reactive. Surface-localized dyes are crucial for applications such as sensing as only this population can interact with the surrounding aqueous medium.[17] Our goal is to determine the CPN size and dye loading that maximize energy transfer efficiency when the sensitized dyes are localized on the particle surface.

Here, we present experimental studies of FRET sensitization of dye dopants in CPNs of 15, 20, and 26 nm diameters. The CPNs are composed of the conjugated polymer poly[(9,9-dioctylfluorenyl-2,7-diyl)-*co*-1,4-benzo-{2,1′-3}-thiadiazole] (PFBT), which is prized for its high fluorescence brightness and photostability. The dye dopants are the photochromic diarylethene 1,2-bis(2,4-dimethyl-5-phenyl-3-thienyl)-3,3,4,4,5,5-hexafluoro-1-cyclopentene (DAE), which switches between open (DAE_o) and closed (DAE_c) forms when irradiated with ultraviolet light and in the reverse direction with visible light (Figure 1). DAE photochromes have attracted

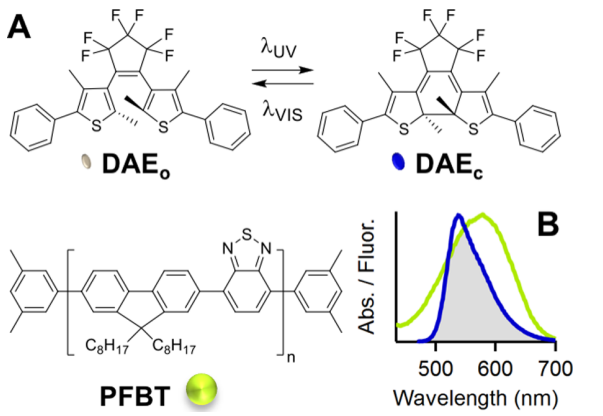

Figure 1. (A) Chemical structures of open (DAE_o) and closed (DAE_c) forms of the DAE dye and the conjugated polymer PFBT. (B) Spectral overlap of the CPN fluorescence spectrum (green) with DAE_c absorbance (blue).

intense attention since their discovery 30 years ago,[41] largely because they exhibit P-type photochromism in which both the colored and colorless forms of the dye are thermally stable.[42] We[22] and others[24−29,33] have shown that CPNs doped with DAEs exhibit fluorescence intensity photomodulation. Here, DAE dyes represent an ideal model for a low-efficiency photochemical reaction as the $DAE_c \rightarrow DAE_o$ cycloreversion has a quantum yield of just 1.5%.[43] The fluorescence spectrum of the donor CPNs and the absorbance spectrum of the acceptor DAE_c share the spectral overlap required for FRET (Figure 1B). The Förster radius (R_0) for the pair is 1.4 nm, which is lower than those of many CPN-dye FRET pairs because of the relatively low extinction coefficient of DAE_c[43] (11,000 M^{-1} cm^{-1}). Colorless DAE_o absorbs only in the ultraviolet region and cannot act as a FRET acceptor for the

https://dx.doi.org/10.1021/acs.jpcc.0c09084
J. Phys. Chem. C 2020, 124, 26474−26485

CPNs. A study of the FRET-sensitized $DAE_c \rightarrow DAE_o$ cycloreversion will enable the determination of the energy transfer efficiency and reaction duration as well as quantification of the antenna effect (AE) of the light-harvesting CPNs.

We studied amplified energy transfer in the DAE-doped CPNs by investigating both fluorescence quenching of CPN donors and sensitization of DAE_c acceptor dyes. Both methods demonstrate that the per-dye energy transfer efficiency decreases with increasing CPN size across the series of 15, 20, and 26 nm particles studied here. Remarkably, DAE_c dyes are able to quench ≥97% of CPN fluorescence in all nanoparticle size populations in spite of their location on the particle surface and the small Förster radius for this FRET pair. The dyes do become less effective quenchers as CPN size increases, with higher dye loadings required to offset the lower per-dye energy transfer efficiencies in larger CPNs. The ability of individual dyes to act as FRET acceptors is highly variable, with some dyes exhibiting exceptional quenching abilities and others acting as poor quenchers or nonquenchers. Photokinetic studies of the DAE_c acceptor dyes demonstrate that the cycloreversion reaction is sensitized in all CPN-size populations, with rate constants 4−32 times faster than those of direct excitation, depending on CPN size and dye loading. Energy-transfer efficiencies are the highest and reaction times are the fastest for 15 nm CPNs, followed by the 20 and 26 nm CPNs. An unexpected thresholding behavior underscores the crucial importance of dye loading: in all CPN-size populations, the energy transfer efficiency increases with DAE_c loading up to a critical concentration, after which it drops abruptly. From these findings, we draw practical recommendations for maximizing the reactivity of inefficient photochemical reactions or photophysical processes through the use of CPN sensitizers.

EXPERIMENTAL METHODS

Materials. All chemicals not listed below were obtained from Acros or Sigma-Aldrich and used as received unless otherwise specified. PFBT with an average molecular weight (MW) of 107,000 and a polydispersity of 3.5 was obtained from American Dye Source (Quebec, Canada). A polystyrene polymer grafted with carboxylic acid-terminated ethylene glycol segments (PS-PEG-COOH) with a total-chain MW of 21,700, a graft side-chain MW of 12,000, a main-chain MW of 8500, and a polydispersity of 1.25 was obtained from Polymer Source Inc. (Quebec, Canada). The photochromic dye DAE was obtained from TCI Chemicals.

Nanoparticle Preparation. CPNs were prepared by a literature procedure.[15] Separate stock solutions of the conjugated polymer PFBT (1 mg/mL), optically transparent stabilizing copolymer PS-PEG-COOH (1 mg/mL), and photochromic DAE dye (2 mg/mL) in anhydrous tetrahydrofuran (THF) were stirred under argon for at least 2 h before use. A precursor solution was prepared by combining portions of the PFBT, PS-PEG-COOH, and DAE solutions with additional THF, as well as varying amounts of ultrapure water to manipulate the particle size,[44,45] to a final concentration of 0.04 mg/mL PFBT, 0.008 mg/mL PS-PEG-COOH, and varying concentrations of the DAE dye depending on the experiment. This precursor solution was filtered through a 0.7 μm filter to remove any aggregates and then sonicated for 30 s to ensure homogeneity. A 1 mL portion of the precursor solution was injected into 8 mL of sonicating ultrapure water, which was then sonicated for an additional 2 min. THF was removed via argon bubbling at 50 °C for 30 min, and the aqueous suspension of DAE-doped CPNs was filtered through 0.7 and 0.22 μm filters. To test for dye leaching, DAE-doped CPNs of each size were spun at 5000 rpm for 2 min in a centrifugal filtration device (Amicon Ultra-4 centrifugal filter with an MW cutoff of 100,000) in accordance with a literature procedure.[46] Nanoparticle size distributions were measured in the aqueous suspension by dynamic light scattering using a Nicomp N3000 Submicron Particle Sizer (Particle Sizing Systems).

Spectroscopy and Photochemistry. Absorption and fluorescence measurements were carried out with an Agilent Technologies Cary 60 UV−vis spectrophotometer and a Varian Eclipse fluorimeter, respectively. All fluorescence experiments used an excitation wavelength of 450 nm. Fluorescence kinetics were monitored at 533 nm. Absorbance kinetics were monitored at 600 nm. CPNs were studied in the aerated aqueous suspension in semimicro quartz cuvettes (Starna, 10 mm × 4 mm interior dimensions). Small sample volumes (250 μL) were used to maximize consistency of the visible irradiation intensity throughout the sample. UV irradiation (254 nm) was provided by a shortwave UV pen lamp (Analytik Jena UVP Pen-Ray Lamp). Visible irradiation (455 or 590 nm) was provided by a 4-wavelength high-power light-emitting diode (LED) source (Thorlabs, DC4100). Irradiation was delivered to the top of the sample cuvette in the absorbance and fluorescence instruments by a liquid light guide (Thorlabs, LLG0538). Photon flux values for 455 and 590 nm irradiation were determined by chemical actinometry[47] using Aberchrome 670.[48]

RESULTS AND DISCUSSION

CPN Design, Preparation, and Properties. DAE-doped PFBT CPNs (Figure 1A) were designed as a model system for FRET sensitization of low-efficiency photochemical reactions by CPNs. The $DAE_c \rightarrow DAE_o$ cycloreversion reaction was selected for study because it has a low quantum yield (1.5 vs 46% for the cyclization reaction)[43] and is induced by visible irradiation, making it amenable to sensitization by CPNs. DAE-doped CPNs were prepared by a reprecipitation method in which a THF solution containing the conjugated polymer, the dye, and an optically transparent stabilizing polymer is injected into sonicating water. Our standard procedure typically produces PFBT CPNs with diameters in the 13−15 nm range. To produce larger CPNs for energy transfer studies, small amounts of water were added to the THF precursor solution prior to injection into water. This method has previously been shown to be effective for producing CPNs of different sizes in a controlled fashion: the CPN diameter increases as the proportion of water in the THF precursor solution increases.[44,45] Size distributions for DAE-doped PFBT CPNs were measured by dynamic light scattering (Figure 2). Precursor solutions that contained 0, 5, and 10% v/v water in THF produced CPNs with average diameters of 15, 20, and 26 nm, respectively. These samples, denoted as CPN_{15}, CPN_{20}, and CPN_{26}, are in the range over which FRET efficiency has previously been shown to increase with increasing particle size when acceptor dyes are doped throughout the particles.[15,16] The size distributions are broad (15 ± 11, 20 ± 13, and 26 ± 15 nm), but the data below show that the three populations demonstrate significant differences in energy transfer behavior. The number of polymer chains per nanoparticle can be estimated from the particle size and the polymer MW as

https://dx.doi.org/10.1021/acs.jpcc.0c09084
J. Phys. Chem. C 2020, 124, 26474−26485

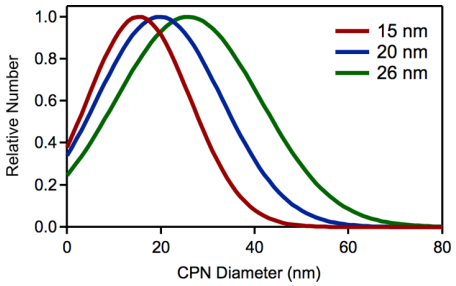

Figure 2. Size distribution of DAE-doped CPNs measured in the aqueous suspension by dynamic light scattering.

described previously.[35] CPN_{15}, CPN_{20}, and CPN_{26} are composed of 8, 19, and 41 polymer chains, respectively. The DAE_c concentrations, calculated from absorbance, are varied throughout this work but have maximum values of 28, 93, and 235 dyes per conjugated polymer chain for CPN_{15}, CPN_{20}, and CPN_{26}, respectively. DAE-doped CPNs were tested for dye leaching by spinning them in a centrifugal filtration device that separates the CPNs from the aqueous medium. The absorbance of the aqueous filtrate was recorded after UV irradiation to produce DAE_c from any DAE_o dyes present. No DAE_c was observed, indicating that the hydrophobic DAE dyes are stably associated with the CPNs.

Dyes in as-prepared CPNs are in the DAE_o form, which does not perturb CPN fluorescence (Figure 3A,B, 1). A brief UV irradiation cyclizes some of the dyes, quenching CPN fluorescence and producing the initial sample for energy transfer studies (Figure 3A,B, 2). DAE_c dyes in the CPN environment absorb between 450 and 700 nm with a λ_{max} of ca. 575 nm (Figure 3C, 2). In the experiments that follow, the duration of UV irradiation was adjusted to produce the desired DAE_c concentration. By varying the irradiation time for different aliquots of the same sample, a set of otherwise identical samples with different DAE_c concentrations was produced. The 1−10 s UV-irradiation times employed here cause 9−28% of DAE_o dyes to convert to DAE_c. For the same irradiation time, conversion increases slightly with CPN size (e.g., 14, 17, and 19% for CPN_{15}, CPN_{20}, and CPN_{26}, respectively, with 4 s of UV irradiation).

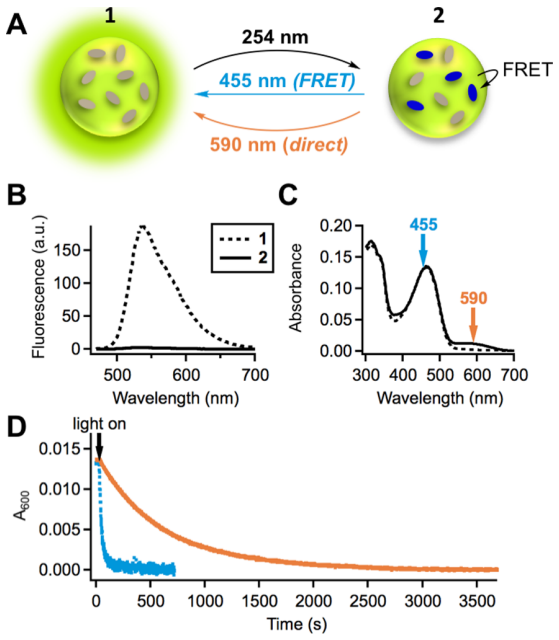

Figure 3. (A) Scheme for operation of DAE-doped CPNs, showing fluorescence on-state with dyes in the DAE_o form (state 1) and off-state with some dyes switched to the quenching DAE_c form (state 2). Fluorescence (B) and absorbance (C) spectra of DAE-doped CPNs as prepared in state 1 and after UV irradiation to produce state 2. (D) Absorbance of DAE_c in DAE-doped CPNs monitored at 600 nm as a function of time during direct excitation (590 nm, orange trace) and FRET-sensitized excitation (455 nm, blue trace) at a photon flux of 1.2×10^{-5} M s^{-1}.

CPNs in state 2 switch to state 1 upon $DAE_c \rightarrow DAE_o$ cycloreversion, which can be induced by either direct or FRET-sensitized pathways. Irradiation with a 590 nm LED induces $DAE_c \rightarrow DAE_o$ without affecting the CPNs, which do not absorb appreciably above 530 nm. Alternatively, the cycloreversion can be induced via the FRET pathway by irradiating into the main CPN absorption band (λ_{max} = 465 nm, Figure 3C) with a 455 nm LED. DAE_c absorbs poorly at this wavelength, and all kinetic data are corrected for the minor amount of direct DAE_c excitation with the blue light. The selection of the direct or FRET-sensitized pathway for cycloreversion has a profound effect on the reaction kinetics. The cycloreversion reaction is easily monitored by tracking the decay of the DAE_c absorbance at 600 nm, which was selected to be far to the red of the CPN absorbance. Figure 3D shows that a sample irradiated at 590 nm (direct pathway) takes far longer (10×) to complete the cycloreversion reaction than the same sample irradiated at 455 nm (FRET pathway) at the same photon flux. The dramatic increase in reaction rate observed in the FRET pathway is consistent with our previous observations in other dye dopants sensitized by CPNs.[35] We previously demonstrated that the exceptional light-harvesting ability of the CPNs and highly efficient energy transfer to dye dopants are responsible for the accelerated reaction kinetics.[35] However, the CPN size and dye loading that maximize this effect remain unknown.

Donor Fluorescence Quenching. CPNs function as a light-harvesting and sensitizing moiety when doped with dyes that can act as energy transfer acceptors. Successful CPN-to-dye energy transfer yields quenched CPN fluorescence, and studying the fluorescence quenching as a function of dye loading can generate insight into the delivery of excitation energy to the dyes. The steady-state energy transfer efficiency is given by $E_{fluor} = 1 - F_{DA}/F_D$, where F_{DA} and F_D are the fluorescence intensities of the CPNs in the presence and absence of DAE_c dye dopants, respectively. We denote this efficiency as E_{fluor} to distinguish it from the efficiency obtained from photokinetic measurements of the dye in the following section. In the CPN environment, E_{fluor} reflects fluorescence quenching from the combination of Förster transfer and exciton diffusion, which can enhance efficiency by delivering excitons to acceptors from distances exceeding the Förster radius. We were able to obtain highly efficient fluorescence quenching in CPNs from all three size populations, with the maximum E_{fluor} > 99% for CPN_{15} and CPN_{20} and E_{fluor} = 97% for CPN_{26} (Figure 4A inset). However, the dye loading required to obtain maximum efficiency increased with increasing CPN size, with CPN_{20} and CPN_{26} requiring 3 and 6 times as many dyes per polymer chain, respectively, to achieve their maximum E_{fluor} relative to CPN_{15}.

https://dx.doi.org/10.1021/acs.jpcc.0c09084
J. Phys. Chem. C 2020, 124, 26474−26485

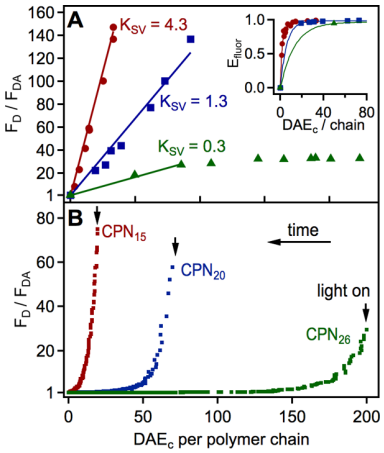

Figure 4. (A) SV plot showing quenching of CPN fluorescence by static populations of DAE$_c$ dyes in 15 (red), 20 (blue), and 26 nm (green) CPNs. Inset: quenching expressed as E_{fluor} vs dye concentration. (B) "Dynamic" SV plot obtained as DAE$_c$ concentration decreases over time during continuous irradiation of doped CPNs at 455 nm.

Stern−Volmer (SV) analysis facilitates a more detailed examination of fluorescence quenching, expressed as $F_D/F_{DA} = 1 + K_{SV}[Q]$, where K_{SV} is the SV constant and [Q] is the molar concentration of the quencher.[49] We divided each CPN sample into multiple aliquots and varied the duration of UV irradiation for each aliquot to produce a set of otherwise identical samples with different DAE$_c$ concentrations. The resulting SV plot (Figure 4A) shows significant differences among the three CPN sizes. The CPN$_{15}$ and CPN$_{20}$ samples yield linear plots, while CPN$_{26}$ increases linearly and then maintains a constant quenching level as dye loading is increased further. The shape of the CPN$_{26}$ plot was consistent across different samples that spanned similar dye loadings, including one sample that had additional data points in the linear region. For other dye-doped CPNs, McNeill has shown that expressing [Q] as the molecular ratio of dyes to conjugated polymer chains enables the determination of the number of polymer chains quenched per dye molecule.[14] Linear fits of CPN$_{15}$, CPN$_{20}$, and the low-concentration portion of the CPN$_{26}$ data give K_{SV} values of 4.3, 1.3, and 0.3, respectively, when the quencher concentration is expressed in dyes per PFBT chain. For CPN$_{15}$, the K_{SV} value indicates that each dye molecule quenches four PFBT molecules on average. Taking into account the volume occupied by this amount of polymer, the K_{SV} value can be translated to an effective quenching radius of 6.1 nm. The same analysis for CPN$_{20}$ and CPN$_{26}$ yields effective quenching radii of 4.1 and 2.5 nm, respectively. For all three size populations, the effective quenching radius exceeds the calculated Förster radius (R_0) of 1.4 nm. It should be noted that R_0 was calculated using the traditional value of 2/3 for the κ^2 orientation factor and should be considered a lower limit as the actual value is often higher in similar systems.[14] Quenching radii that exceed R_0 have been interpreted as a sign of exciton diffusion in other dye-doped CPNs.[14]

Several features of the SV analysis indicate that the DAE$_c$ dyes are located on or near the CPN surface. Collectively, the amount of dye required to obtain maximum fluorescence quenching, the K_{SV} values, and the effective quenching radii indicate that DAE$_c$ dyes become less effective fluorescence quenchers as the CPN size increases. Indeed, the CPN$_{26}$ data show that a fluorescence quenching ceiling is reached, and no amount of additional dye will yield larger F_D/F_{DA} values past a certain point. These results are consistent with surface-localized dyes: as CPN size increases, the probability that a given exciton will be close enough to the surface to be quenched by a dye decreases. We previously used solvatochromic data to show that only surface-localized dyes were able to undergo a photochromic reaction in spirooxazine-doped CPNs.[23] The fluorescence quenching data indicate that a similar photoselection process is at work here, with dyes not near the surface remaining in their nonquenching DAE$_o$ form. The DAE cyclization reaction has been previously shown to occur with a reduced quantum yield (or not at all) in polymer films.[50] Kwon et al. found that the DAE cyclization quantum yield decreased as polymers with increasingly high glass-transition temperatures (T_g) were used as the host matrix and attributed this result to the small free-volume voids in rigid polymers.[50] Although the rigidity of the nanoparticle environment is not known, McNeill has previously found that polyfluorene CPNs exhibit properties consistent with a glassy polymer phase.[51] The PFBT conjugated polymer used in the present work has a higher T_g (112 °C)[52] than the most rigid polymer studied by Kwon.

The SV data in Figure 4A were drawn from absorption and fluorescence spectra of sample aliquots with varying amounts of DAE$_c$ quenchers produced by UV irradiation. Each data point represents fluorescence quenching by a static population of DAE$_c$ dyes. After finding it difficult to create samples with low DAE$_c$ concentrations in larger CPNs with this method, we produced a second set of SV plots for which we varied the DAE$_c$ concentration as a function of time with continuous irradiation. CPN samples were UV-irradiated to produce a significant amount of DAE$_c$ and divided into two aliquots, each of which was irradiated with 455 nm to induce DAE$_c$ → DAE$_o$ cycloreversion via the FRET pathway, while absorbance values and fluorescence intensities were recorded as a function of time. The absorbance and fluorescence traces were synchronized in time to produce "dynamic" SV plots, all of which are nonlinear with an upward curvature (Figure 4B). Single exponential fits fail to reproduce the observed curvature, particularly for CPN$_{20}$ and CPN$_{26}$. All curves show sharp declines in F_D/F_{DA} at the beginning of the experiment when high DAE$_c$ concentrations are present and a gradual leveling out as the dye concentration continues to decrease over time. Additionally, the CPN$_{20}$ and CPN$_{26}$ plots exhibit flat tails when DAE$_c$ concentrations are low, reflecting a concentration regime where the dyes are apparently ineffective for fluorescence quenching.

Many different mechanistic and sample-specific phenomena are known to produce nonlinear SV plots.[49] For example, conjugated polyelectrolytes exhibit upward-curving SV plots because of quencher-induced aggregation.[53,54] In the case of CPNs quenched by FRET, upward-curving SV plots have been observed by McNeill when a conjugated polymer acts as the acceptor and the FRET efficiency is extremely high.[55,56] The curvature was reproduced by a model that assumed a Poissonian distribution of polymeric acceptors and yielded a quenching efficiency of 99%.[56] This model failed to reproduce our data, likely because it employs a single value for the quenching efficiency per acceptor. We hypothesize that the per-dye FRET efficiency in the DAE$_c$-doped CPNs is highly variable, with some dyes acting as powerful fluorescence quenchers and others as more modest quenchers or even

https://dx.doi.org/10.1021/acs.jpcc.0c09084
J. Phys. Chem. C 2020, 124, 26474−26485

nonquenchers. These dyes likely vary in their location and/or orientation, which impact energy transfer[57] through the donor−acceptor distance and the κ^2 orientation factor. Because cycloreversion is induced by FRET sensitization of DAE_c, dyes with high FRET efficiencies are more likely to undergo cycloreversion first. This photoselection process increases the proportion of poor quenchers in the dye ensemble as the experiment proceeds in time, a phenomenon that has been observed previously in DAE-labeled quantum dots.[58]

The impact of photoselection on fluorescence quenching in DAE_c-doped CPNs can be examined through three representative dye populations for each sample: efficient quenchers, poor quenchers, and nonquenchers. The quenching power of the efficient and poor quenchers can be estimated by performing linear fits of small regions of the SV plot. The efficient quenchers are represented by the first 10% of the dyes to undergo switching after the light is turned on, while the poor quenchers are represented by the 10% of the dyes bounded on the low-concentration end by the point where $F_{DA}/F_D = 1.5$. Nonquenchers are defined as those that do not affect fluorescence intensity ($F_{DA}/F_D < 1.1$). These dyes are still able to undergo the cycloreversion reaction, albeit inefficiently, via direct excitation by the 455 nm irradiation. CPN_{15} has no nonquenching dyes and yields K_{SV} values of 11.0 and 0.33 for the efficient and poor quenchers, respectively. These values translate to quenching radii of 8.4 and 2.6 nm. Efficient quenchers in these smaller CPNs may be able to quench nearly all the fluorescence in a particle, while even the poor quenchers exhibit a quenching radius that exceeds the Förster radius. In contrast, 10% of the dyes in CPN_{20} are nonquenching, and K_{SV} values for efficient (5.5) and poor (0.050) quenchers are lower than those for CPN_{15}. The K_{SV} value for the poor quenchers translates to a 1.4 nm radius, which is identical to the Förster radius for this system. It is possible that the poor quenchers are able to undergo Förster transfer but are in a location that is not accessible by exciton diffusion pathways. As expected, CPN_{26} has the most nonquenchers at 40% of the total dye population for this particular sample. K_{SV} values for the poor quenchers match those for CPN_{20} (0.055), while K_{SV} values for the efficient quenchers are significantly lower than those for CPN_{20} (0.94). For all three CPN-size populations, K_{SV} values for the efficient quenchers exceed those from the SV plots in Figure 4A, which reflect the aggregate quenching power of the entire static DAE_c ensemble rather than the photoselected subsensembles in the present analysis.

From the SV analysis, we can conclude that it is possible to achieve highly efficient quenching of CPN fluorescence in all three nanoparticle-size populations but that DAE_c dyes become less effective quenchers as CPN size increases. The dynamic SV plots further indicate that individual dyes vary dramatically in their ability to quench fluorescence. Our original goal was to determine the CPN size and composition that maximize FRET efficiency to dye dopants for the purpose of amplifying dye reactivity. While the SV analysis indicates that dyes in CPN_{15} are the most efficient fluorescence quenchers, it does not reveal the dye loading that will maximize reactivity of the dyes. A more detailed and nuanced view of energy transfer in this system can be obtained by studying the acceptor dyes themselves. Photokinetic methods have previously been used to study acceptor heterogeneity in multiple-acceptor FRET systems[58,59] and will enable us to examine dye sensitization as a function of CPN size and dye loading.

Acceptor Cycloreversion Sensitization. DAE reaction kinetics has been studied extensively in a variety of environments, with recent examples including solution,[60,61] metal−organic frameworks,[62,63] and quantum dots.[58] Here, we studied the $DAE_c \rightarrow DAE_o$ cycloreversion under continuous irradiation to obtain the energy transfer efficiency and to probe its dependence on CPN size and dye loading. The photochromic reaction represents a simple equilibrium between the forward cyclization reaction (k_1, eq 1) and the cycloreversion reaction (k_2). We monitored the absorbance of DAE_c under continuous visible irradiation at wavelengths that do not induce the forward reaction (455 or 590 nm). The differential rate law for the disappearance of DAE_c upon direct excitation involves only the cycloreversion reaction and is given by eq 2[64,65]

$$DAE_o \underset{k_2}{\overset{k_1}{\rightleftharpoons}} DAE_c \tag{1}$$

$$-\frac{d[DAE_c]}{dt} = I_0 F_\lambda \varepsilon_\lambda l \Phi_{c\rightarrow o}[DAE_c] \tag{2}$$

where I_0 is the incident photon flux, F is the photokinetic factor at the irradiation wavelength λ ($F = [1 - 10^{-Abs_\lambda}]/Abs_\lambda$), ε_λ is the extinction coefficient of DAE_c at the irradiation wavelength λ, l is the path length, and $\Phi_{c\rightarrow o}$ is the quantum yield of the cycloreversion reaction. We can define k_2, the cycloreversion rate constant upon direct excitation, according to eq 3

$$k_2 = I_0 F_\lambda \varepsilon_\lambda l \Phi_{c\rightarrow o} \tag{3}$$

We studied direct excitation of DAE_c at 590 nm in all three CPN-size populations as a function of I_0 and obtained k_2 values from fits of the kinetic decays. The cycloreversion rate constant k_2 increases linearly with I_0, as expected from eq 3 (Figure 5).

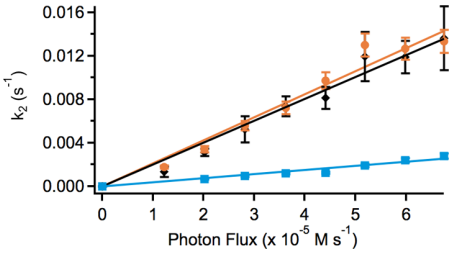

Figure 5. Rate constant for cycloreversion vs input photon flux for direct excitation of DAE_c dyes in CPNs at 590 nm (orange) and in THF solution at 590 nm (black) and 455 nm (blue).

All three sets of CPNs gave virtually identical rate constants, with any differences within the experimental error. These data are thus shown as an average for the CPN environment in Figure 5. The fact that k_2 is independent of CPN size is expected because the CPNs cannot absorb the 590 nm irradiation and thus function as an inert medium for the dyes in this experiment. To provide context for the behavior of the dye in CPNs, k_2 values were also measured for direct excitation of the dye in THF solution at both 590 and 455 nm (Figure 5). Within the error, DAE_c's response to direct excitation at 590 nm is identical in THF and CPN environments, a finding that provides further evidence that DAE_c dyes are located on the

https://dx.doi.org/10.1021/acs.jpcc.0c09084
J. Phys. Chem. C 2020, 124, 26474−26485

nanoparticle surface. As expected, given DAE_c's poor absorbance at 455 nm, the cycloreversion reaction is much slower when induced by blue light. Because the cycloreversion quantum yield is the only unknown in eq 3, it can be calculated from the slopes of the lines of Figure 5. All three lines yield a $\Phi_{c\rightarrow o}$ value of 1%. This value is slightly lower than literature values for DAE_c in hexane solution[43,66] but is consistent with the fact that the cycloreversion quantum yield decreases with increasing solvent polarity for related DAE dyes.[67]

When CPNs with dyes in the DAE_c form are irradiated with blue light, >99% of the light is absorbed by the CPNs, which can then transfer the energy to the dyes via the combination of Förster transfer and exciton diffusion. FRET sensitization of the cycloreversion reaction adds an additional pathway to the differential rate law (eq 4)

$$-\frac{d[DAE_c]}{dt} = k_2[DAE_c] + I_0F_{455}\varepsilon_{CPN,455}l[CPN]\Phi_{c\rightarrow o}E_{kin} \quad (4)$$

where the first and second terms represent direct and FRET excitation of the dye at 455 nm, respectively, and E_{kin} is the energy transfer efficiency in the photokinetic experiment. Although both E_{fluor} and E_{kin} represent energy transfer efficiencies, we will continue to use distinct symbols to designate the origin of each measurement. The FRET term dominates the reaction kinetics as the relevant extinction coefficient is now that of the CPN, which varies with CPN size and is approximately 400, 900, and 2000 times larger than that of DAE_c for 15, 20, and 26 nm CPNs, respectively. It is important to note that E_{kin} is not a fixed value for each sample. Both the SV analysis above (Figure 4) and the literature precedent for DAE-functionalized quantum dots by Jovin and co-workers[58] demonstrate that E_{kin} varies in time because of photoselection. Here, we extracted the initial value of E_{kin} from photokinetic data for samples of different initial dye concentrations to determine the optimal composition and size of DAE-doped CPNs. For each CPN size population and a range of dye concentrations, we recorded kinetic traces of the absorbance as the DAE_c population decayed under continuous irradiation at 455 nm (see the sample trace, Figure 3D). All kinetic traces were recorded with the same low value for the 455 nm photon flux (1.2×10^{-5} M s^{-1}) to prevent the reaction from occurring faster than the time resolution of the instrument and to reduce the probability of photobleaching. Selection of dye concentration ranges was guided by fluorescence quenching data: the highest dye concentrations studied were those that yielded the maximum fluorescence quenching (E_{fluor} > 99% for CPN_{15} and CPN_{20} and E_{fluor} = 97% for CPN_{26}), while the lowest were those in which the signal-to-noise ratio of the absorbance traces remained sufficient for data analysis. To extract E_{kin}, the first several seconds of each absorbance kinetic trace were fit with a curve, which was converted to dye concentration using Beer's law and differentiated with respect to time. E_{kin} was then calculated from $d[DAE_c]/dt$ as the remaining terms in eq 4 are all known. Given that the DAE_c dyes appear to be on the CPN surface, E_{kin} values were plotted as a function of dye concentration in units of dyes per nm^2 of CPN surface area to facilitate comparison among the three CPN-size populations.

The initial E_{kin} values exhibit an unexpected threshold behavior as dye loading is increased (Figure 6A–C). For both CPN_{15} (A) and CPN_{20} (B), E_{kin} increases with increasing DAE_c concentration up to a point, after which a sharp decline

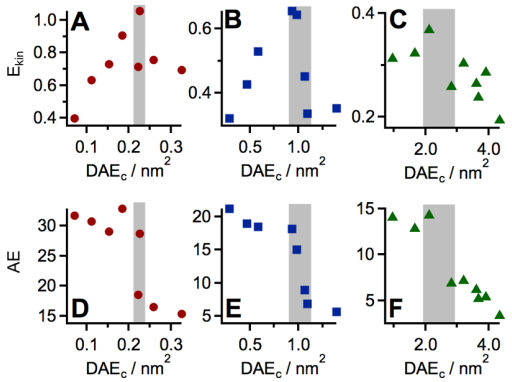

Figure 6. Energy transfer efficiency (E_{kin}) and the AE obtained from photokinetic measurements as a function of DAE_c dyes per nm^2 of CPN surface area for 15 (A,D), 20 (B,E), and 26 nm (C,F) CPNs.

and leveling out are observed. In the low-concentration regime, the increase in E_{kin} with concentration mimics the trend observed for E_{fluor}, which reports on energy transfer efficiency from the donor perspective (see the inset of Figure 4A). In this concentration regime, individual dyes are sparse enough that they do not compete with each other for excitons, so E_{kin} increases as the number of acceptor dyes increases in a similar manner to E_{fluor}. Once E_{fluor} reaches its maximum value, it remains constant as additional dyes are added (Figure 4A). In contrast, E_{kin} plummets, dropping from 100 to 70% in CPN_{15} and from 66 to 34% in CPN_{20} in the concentration regimes highlighted by the gray boxes in Figure 6. We attribute the drop in E_{kin} values to two factors. First, as dye concentration increases, eventually there are so many dyes that they must compete with each other for CPN excitons. The average per-dye energy transfer efficiency drops because the dye concentration exceeds that required for capturing the energy of all excitons. Second, as dye loading is increased to fairly high levels, it is likely that the number of poorly quenching or nonquenching dyes in the ensemble also increases. E_{kin} is sensitive to both these factors because it reports on the acceptor population as a whole, whereas E_{fluor} reports only on the quenching of donor excitons and thus remains constant once maximum quenching is reached. We had hypothesized that E_{kin} would decline in the high-concentration regime for these reasons but did not anticipate the abrupt transition observed here. The transition appears to occur over a wider concentration range as CPN size increases. This trend is particularly apparent in CPN_{26}, where the transition occurs over such a wide range of dye concentrations that it is unclear whether the same type of transition is truly present.

The initial E_{kin} values in Figure 6 facilitate a comparison of the energy transfer efficiency across the three CPN-size populations. E_{kin} decreases as CPN size increases, with maximum E_{kin} values of 100, 66, and 37% for 15, 20, and 26 nm CPNs, respectively. The 100% value observed for CPN_{15} is consistent with the E_{fluor} value of 98% obtained at the same dye loading and suggests that all energy harvested by the CPNs is transferred to the DAE_c acceptor dyes in this sample. The maximum E_{kin} values for CPN_{20} and CPN_{26} are significantly lower than E_{fluor} values obtained at the same dye loadings, 98% for CPN_{20} and 96% for CPN_{26}. This apparent contradiction is due to the influence of poorly quenching and nonquenching acceptor dyes on the DAE_c decay kinetics in CPN_{20} and CPN_{26}. All dyes in the ensemble affect the E_{kin} value, while

https://dx.doi.org/10.1021/acs.jpcc.0c09084
J. Phys. Chem. C 2020, 124, 26474–26485

E_{fluor} is sensitive only to the disappearance of CPN excitons as they are quenched. In the larger CPN sizes, achieving maximum energy transfer efficiency requires high dye loadings that include poorly quenching and nonquenching dyes in all samples. This point will be considered in more detail further below. For all three CPN sample sizes, the dye loading at which E_{kin} is maximized coincides with an E_{fluor} value 1% lower than the maximum observed for that sample at higher dye loadings. This relationship provides a useful guideline for determining the optimal dye loading without performing photokinetic studies.

The E_{kin} analysis demonstrates that it is possible to transfer 100% of the energy absorbed by the CPNs to dyes but does not illuminate the extent to which dye reactivity is enhanced as a result. The light-harvesting ability in energy transfer systems is typically quantified by the AE. The AE is frequently reported for systems in which the acceptor dye is fluorescent. In these cases, AE is the ratio of the fluorescence intensity of the dye when excited via energy transfer to that when it is excited directly.[68] For the nonfluorescent acceptor dyes studied here, we can obtain the same information from the ratio of rate constants for the photochromic reaction. We define AE as k_{FRET}/k_2, where k_{FRET} is the initial rate constant for the $DAE_c \rightarrow DAE_o$ reaction during 455 nm irradiation (FRET pathway) and k_2 is the rate constant for the same reaction during 590 nm irradiation (direct pathway). The AE values for all CPN-size populations are greater than unity, demonstrating that the photochromic reaction is accelerated when sensitized by the CPNs in all systems studied here (Figure 6D−F). AE values are high and relatively constant at low dye loadings and plummet in abrupt fashion analogous to the E_{kin} values once the threshold region is reached. The maximum AE values are 32 for CPN_{15}, 19 for CPN_{20}, and 14 for CPN_{26}. These high values indicate that the CPNs are exceptional sensitizers for the photochromic reaction of DAE dyes, which here serve as a model system for dyes that undergo low-quantum-yield photochemical reactions. Our AE values are consistent with those reported in the literature for CPNs that undergo energy transfer to fluorescent acceptor dyes, which range from 5 to 31.[69,70]

The AEs documented above demonstrate that CPNs are useful sensitizers for low-quantum-yield photochemical reactions. If we are to apply these findings to other dyes, then the reaction duration becomes an important practical consideration. We determined the time required for half of the DAE_c dyes in a sample to react (halftime, $t_{1/2}$) from the absorbance decays recorded under continuous 455 nm irradiation (Figure 7A−C). The halftime values for all samples are lower than that obtained upon direct excitation of the dye on the CPNs with 590 nm light (ca. 400 s, Figure 3D). The sensitized reaction slows as the CPN size increases, which is consistent with the observed decrease of initial E_{kin} and AE values with increasing CPN size. For a given CPN size, the reaction is the fastest at low dye concentrations, where individual dyes do not compete with each other for CPN excitons. A sudden slowing of the reaction occurs at the same dye concentration as the thresholds for the E_{kin} and AE values. The abrupt increase is particularly apparent for CPN_{15} and CPN_{20} and, as above, less so for CPN_{26}, which appears to exhibit a more continuous change in halftime values. The consistent observation of the threshold behavior in Figures 6 and 7 is noteworthy because the halftime values are obtained from a simple measurement that does not rely on any assumptions about the rate law or energy transfer processes. Thus, they serve as a cross-check on the E_{kin} and AE analyses above. The halftime analysis also underscores the critical importance of dye loading for CPN-sensitized photochemical reactions. The CPN_{15} sample with the highest dye loading has a longer halftime (32 s) than the CPN_{20} and CPN_{26} samples with the lowest dye loadings (19 s). Preparing CPNs with dye concentrations below the threshold value is important for experiments in which reaction duration is a concern. Reaction duration can also be manipulated by changing the irradiation intensity, and thoughtful balancing of CPN size, dye loading, and irradiation intensity can be used to achieve a target duration if desired.

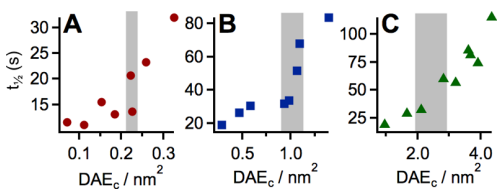

Figure 7. Time for half of the DAE_c dyes in doped CPNs to complete the cycloreversion reaction as a function of initial dye loading for 15 (A), 20 (B), and 26 nm (C) CPNs.

The halftime data highlight the crucial importance of initial dye concentration in the operation of CPN sensitizers. A dye-doped CPN sample with an initial dye concentration above the threshold will react slowly and exhibit values for initial AE and E_{kin} that are significantly lower than the maximum possible values for its CPN size (Figures 6 and 7). For a CPN system under continuous irradiation, the evolution of energy transfer efficiency in time is dictated by the initial energy transfer efficiency. Because of the photoselection phenomenon that removes the dyes with the highest per-dye efficiencies from the ensemble first, doped CPNs with initial dye concentrations above the threshold will never exhibit the high E_{kin} values observed at lower dye loadings, even when they pass through the same concentration regime in time.

The impact of photoselection is demonstrated in Figure 8, which shows dynamic SV plots as a function of dye concentration for three CPN_{20} samples with different initial dye loadings. As for the size-dependent plots in Figure 4B, the graphs were obtained from kinetic traces of absorbance and fluorescence during continuous irradiation at 455 nm to activate the FRET pathway. The maximum E_{kin} values for CPN_{20} were observed at a dye loading of 0.93 dyes/nm^2 of particle surface area, equivalent to 62 dyes per polymer chain and marked with a dashed line in the figure. The initial E_{kin}

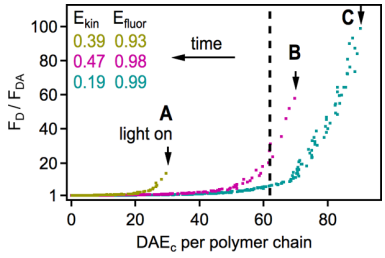

Figure 8. Dynamic SV plots for three samples of 20 nm doped CPNs with different initial dye loadings. The dashed line represents the dye loading at which the maximum E_{kin} is observed.

https://dx.doi.org/10.1021/acs.jpcc.0c09084
J. Phys. Chem. C 2020, 124, 26474−26485

value for each sample determines its trajectory. Sample B, for example, starts just above the line and has an initial E_{kin} value of 0.47. When it reaches the line, it has a dye population equal to that which yields the maximum E_{kin} in Figure 6B. However, the SV plot does not exhibit an increase in quenching at this point because the dyes with the highest per-dye energy transfer efficiencies have already been depleted from the ensemble because of photoselection. The impact of photoselection can be seen even more clearly in sample C, which drops from F_D/F_{DA} = 99 initially to 6.5 at the threshold, indicating the loss of the most powerfully quenching dyes. Figure 8 also shows that all three CPN_{20} samples possess nonquenching dyes. In sample A, which has an initial dye concentration far below the threshold, 16% of dyes are nonquenching. Although the absolute number of nonquenching dyes increases upon moving to sample B, the percentage actually drops to 10%. These results indicate that some dyes will always be unable to quench fluorescence in the larger 20 and 26 nm CPNs.

With the results of Figure 8 in mind, we can now interpret the threshold behavior demonstrated in Figures 6 and 7. For CPN_{15}, which has no nonquenching dyes, the dye loading that generates the maximum E_{kin} likely represents the saturation of the particle surface with the maximum number of dyes that can be present without having to compete with each other for excitons. For CPN_{20} and CPN_{26}, some dyes are nonquenching, even at low dye loadings. Thus, for larger CPNs, the dye loading at the maximum E_{kin} value reflects the saturation of the particle surface with effective quenchers. We wondered whether the nonquenching dyes in CPN_{20} and CPN_{26} might be ineffective FRET acceptors because they are aggregated. Difference spectra created by subtracting the CPN absorbance from that of the DAE_c-doped CPNs are shown in Figure 9A. Although the effect is quite subtle, the DAE_c λ_{max} shifts to blue as CPN size increases, from 578 nm in CPN_{15} to 573 nm in CPN_{26}. Sun and co-workers studied aggregates of a related DAE dye and found that the dyes formed H-aggregates with blue-shifted absorbance.[71] If H-aggregates are present in CPN_{20} and CPN_{26} and act as poor FRET acceptors, then they should be the last subpopulation of the dye to switch back to DAE_o because of photoselection. We irradiated a sample of DAE_c-doped CPN_{26} with 455 nm to activate the FRET pathway and paused at regular intervals during the irradiation to record absorbance spectra. The peak of each absorbance difference spectrum was fit with a Gaussian to obtain the DAE_c λ_{max} (Figure 9B). The λ_{max} clearly shifts to blue as the experiment proceeds, and the spectra also become broader and less Gaussian, as indicated by the larger fit errors for the low-concentration spectra. Figure 9C shows representative high- and low-concentration spectra that illustrate these differences. The shape of the low-concentration spectrum can be reproduced as the sum of two Gaussians, one at 579 nm, which is similar to the dye λ_{max} in DAE_{15}, and the other at 545 nm, which is consistent with H-aggregates. These results support the hypothesis that the nonquenching dyes in the larger CPNs are H-aggregates that are ineffective FRET acceptors.

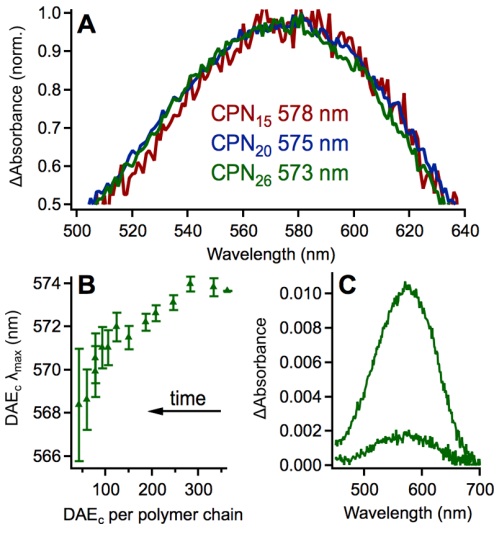

Figure 9. (A) Peaks of difference spectra showing absorbance of DAE_c dyes in the CPN environment and λ_{max} values from Gaussian fits. (B) DAE_c λ_{max} values obtained from Gaussian fits of difference spectra obtained at regular intervals during continuous irradiation of a CPN_{26} sample. (C) Representative high- and low-concentration difference spectra from which (B) was obtained.

CPN Design Recommendations. We can now synthesize the results of these studies to produce design guidelines for CPNs doped with surface-localized photoresponsive dyes. The desired characteristics of a CPN sensitizer will vary depending on the desired outcome:

(1) *Efficient and rapid dye reaction.* To maximize FRET efficiency and minimize reaction duration, 15 nm diameter CPNs are recommended. These CPNs are large enough to fully take advantage of exciton diffusion and exhibit the most amplified FRET, yielding effective quenching radii that exceed the Förster radius. In our studies, CPN_{15} samples did not have any nonquenching dyes that would slow the reaction kinetics nor was there any evidence of the formation of H-aggregates. Optimal dye loading is that which yields an E_{fluor} value of 1% less than the maximum.

(2) *Highest concentration of the dye photoproduct.* If the sensitized reaction is intended to deliver a small molecule to the surrounding medium (e.g., through photochemical bond cleavage), then small CPNs may not yield as much photoproduct as desired. Higher concentrations of the photoproduct can be delivered by utilizing larger CPNs that can accommodate higher dye loadings. Fluorescence quenching should be monitored to verify that sensitization will be a viable pathway. For our system, CPNs much larger than CPN_{26} would fail to be efficient sensitizers. As mentioned above, optimal dye loading is that which yields an E_{fluor} value of 1% less than the maximum. Long reaction times can be reduced by increasing light intensity provided that the dye dopant does not have an efficient photobleaching pathway.

(3) *CPN fluorescence quenching and/or sensitized acceptor fluorescence.* Our focus here was on using CPNs to sensitize the photochemical reactions of dyes. However, many applications of dye-doped CPNs continue to focus on CPN fluorescence quenching and/or sensitized acceptor fluorescence. For such applications, CPN_{15} would yield the most highly quenched fluorescence and the most amplified acceptor fluorescence. Dye loading would need to be sufficient to quench all CPN fluorescence, but exceeding this amount would not have the same negative consequences that it does for

https://dx.doi.org/10.1021/acs.jpcc.0c09084
J. Phys. Chem. C 2020, 124, 26474−26485

applications in which the output is a photoproduct. In fluorescence-based applications, any surplus, nonquenching dyes would simply act as silent spectators.

The DAE dyes employed here as a model system for an inefficient photochemical reaction are not ideal FRET acceptors because of the low extinction coefficient of DAE_c. A dye dopant with a significantly higher extinction coefficient would have a larger Förster radius and would exhibit higher per-dye FRET efficiencies as compared to DAE_c. Thus, the same levels of fluorescence quenching could be obtained at much lower dye loadings than for DAE_c, and the threshold above which E_{kin} plummets would be correspondingly shifted to lower values. Shifting to lower dye loadings would also reduce the probability of aggregate formation. The optimal CPN size for maximizing amplified FRET would likely shift to larger sizes as well because of the greater quenching power of dyes with large extinction coefficients. The recommendation to tune the dye concentration to that which yields E_{fluor} 1% below the maximum should continue to provide a useful general guideline.

CONCLUSIONS

DAE cycloreversion was employed as a model reaction to study FRET sensitization of inefficient photoreactions by CPNs. Dyes that switch from the nonquenching DAE_o form to the quenching DAE_c form in response to UV light are localized on the nanoparticle surface. The DAE_c dyes effectively quench the fluorescence of CPNs with 15, 20, and 26 nm diameters. However, the dye loading required to obtain highly quenched fluorescence increases with CPN size. High dye loadings come with the risk of aggregate formation, which was observed here in the 20 and 26 nm particles. Dyes in all three CPN sizes show the effects of amplified FRET: they react more rapidly when sensitized by the CPNs than when excited directly and exhibit AEs ranging from 4 to 32. The magnitude of these effects depends on both particle size and dye loading. The 15 nm CPNs exhibit the most amplified FRET, as marked by the greatest AEs and the shortest reaction times. For a given CPN size, reaction times are the shortest and AEs are the greatest at low dye loadings; at a critical dye concentration, an abrupt transition to longer reaction times and reduced AEs is observed. The critical dye concentration can be interpreted as the dye loading at which the CPN surface is saturated with acceptor dyes such that all excitons can be quenched without the dyes competing against each other for excitons. It is at this critical dye concentration that the energy transfer efficiency reaches its maximum for a given CPN size. For all CPN sizes and at all dye concentrations, the FRET-accepting ability of individual dyes varies tremendously. Photoselection reveals this phenomenon as the dyes are selectively depleted from the ensemble in the order of FRET-accepting ability. However, it is extremely important to note that the observation of variable FRET-accepting ability within a dye ensemble is not applicable only to photochromic dyes. Rather, photoselection reveals aspects of dye behavior that likely impact all surface-localized dyes in CPNs but would be difficult to detect if only conventional fluorescent dyes were studied as acceptors. The results are translated to application-dependent design recommendations for dye-doped CPNs.

AUTHOR INFORMATION

Corresponding Author

Elizabeth J. Harbron − *Department of Chemistry, William & Mary, Williamsburg, Virginia 23187-8795, United States;* orcid.org/0000-0003-3339-5451; Email: ejharb@wm.edu

Authors

Lisa S. Graves − *Department of Chemistry, William & Mary, Williamsburg, Virginia 23187-8795, United States*

Matthew J. Goodwin − *Department of Chemistry, William & Mary, Williamsburg, Virginia 23187-8795, United States*

Isabelle N. Maricar − *Department of Chemistry, William & Mary, Williamsburg, Virginia 23187-8795, United States*

Jaclyn A. Rebstock − *Department of Chemistry, William & Mary, Williamsburg, Virginia 23187-8795, United States*

Complete contact information is available at: https://pubs.acs.org/10.1021/acs.jpcc.0c09084

Author Contributions

†L.S.G. and M.J.G. contributed equally.

Notes

The authors declare no competing financial interest.

ACKNOWLEDGMENTS

We gratefully acknowledge support of this work by the NSF (CHE-1856142).

REFERENCES

(1) Klán, P.; Šolomek, T.; Bochet, C. G.; Blanc, A.; Givens, R.; Rubina, M.; Popik, V.; Kostikov, A.; Wirz, J. Photoremovable Protecting Groups in Chemistry and Biology: Reaction Mechanisms and Efficacy. *Chem. Rev.* **2013**, *113*, 119−191.

(2) Ko, C.-C.; Yam, V. W.-W. Coordination Compounds with Photochromic Ligands: Ready Tunability and Visible Light-Sensitized Photochromism. *Acc. Chem. Res.* **2018**, *51*, 149−159.

(3) Papper, V.; Likhtenshtein, G. I. Substituted Stilbenes: A New View on Well-Known Systems: New Applications in Chemistry and Biophysics. *J. Photochem. Photobiol., A* **2001**, *140*, 39−52.

(4) El-Khouly, M. E.; Fukuzumi, S.; D'Souza, F. Photosynthetic Antenna-Reaction Center Mimicry by Using Boron Dipyrromethene Sensitizers. *ChemPhysChem* **2014**, *15*, 30−47.

(5) Yu, J.; Rong, Y.; Kuo, C.-T.; Zhou, X.-H.; Chiu, D. T. Recent Advances in the Development of Highly Luminescent Semiconducting Polymer Dots and Nanoparticles for Biological Imaging and Medicine. *Anal. Chem.* **2017**, *89*, 42−56.

(6) Guo, L.; Ge, J.; Wang, P. Polymer Dots as Effective Phototheranostic Agents. *Photochem. Photobiol.* **2018**, *94*, 916−934.

(7) Gao, D.; Hu, D.; Liu, X.; Zhang, X.; Yuan, Z.; Sheng, Z.; Zheng, H. Recent Advances in Conjugated Polymer Nanoparticles for NIR-II Imaging and Therapy. *ACS Appl. Polym. Mater.* **2020**, *2*, 4241−4257.

(8) Kuehne, A. J. C. Conjugated Polymer Nanoparticles toward In Vivo Theranostics—Focus on Targeting, Imaging, Therapy, and the Importance of Clearance. *Adv. Biosyst.* **2017**, *1*, 1700100.

(9) Abelha, T. F.; Dreiss, C. A.; Green, M. A.; Dailey, L. A.; Abelha, T. F. Conjugated Polymers as Nanoparticle Probes for Fluorescence and Photoacoustic Imaging. *J. Mater. Chem. B* **2020**, *8*, 592−606.

(10) Li, J.; Rao, J.; Pu, K. Recent Progress on Semiconducting Polymer Nanoparticles for Molecular Imaging and Cancer Phototherapy. *Biomaterials* **2018**, *155*, 217−235.

(11) Wang, Y.; Feng, L.; Wang, S. Conjugated Polymer Nanoparticles for Imaging, Cell Activity Regulation, and Therapy. *Adv. Funct. Mater.* **2019**, *29*, 1806818.

(12) Massey, M.; Wu, M.; Conroy, E. M.; Algar, W. R. Mind Your P's and Q's: The Coming of Age of Semiconducting Polymer Dots

and Semiconductor Quantum Dots in Biological Applications. *Curr. Opin. Biotechnol.* **2015**, *34*, 30−40.
(13) Jiang, Y.; McNeill, J. Light-Harvesting and Amplified Energy Transfer in Conjugated Polymer Nanoparticles. *Chem. Rev.* **2017**, *117*, 838−859.
(14) Groff, L. C.; Wang, X.; Mcneill, J. D. Measurement of Exciton Transport in Conjugated Polymer Nanoparticles. *J. Phys. Chem. C* **2013**, *117*, 25748−25755.
(15) Wu, C.; Zheng, Y.; Szymanski, C.; McNeill, J. Energy Transfer in a Nanoscale Multichromophoric System: Fluorescent Dye-Doped Conjugated Polymer Nanoparticles. *J. Phys. Chem. C* **2008**, *112*, 1772−1781.
(16) Wang, S.; Thorn, A.; Redmond, G. Photophysical Probing of Dye Microenvironment, Diffusion Dynamics, and Energy Transfer. *J. Phys. Chem. C* **2018**, *122*, 6900−6911.
(17) Lix, K.; Krause, K. D.; Kim, H.; Algar, W. R. Investigation of the Energy Transfer Mechanism Between Semiconducting Polymer Dots and Organic Dyes. *J. Phys. Chem. C* **2020**, *124*, 17387−17400.
(18) Tian, Z.; Yu, J.; Wu, C.; Szymanski, C.; McNeill, J. Amplified Energy Transfer in Conjugated Polymer Nanoparticle Tags and Sensors. *Nanoscale* **2010**, *2*, 1999−2011.
(19) Chan, Y.-H.; Wu, P.-J. Semiconducting Polymer Nanoparticles as Fluorescent Probes for Biological Imaging and Sensing. *Part. Part. Syst. Charact.* **2015**, *32*, 11−28.
(20) Lyu, Y.; Pu, K. Recent Advances of Activatable Molecular Probes Based on Semiconducting Polymer Nanoparticles in Sensing and Imaging. *Adv. Sci.* **2017**, *4*, 1600481.
(21) Zhang, X.; Chamberlayne, C. F.; Kurimoto, A.; Frank, N. L.; Harbron, E. J. Visible Light Photoswitching of Conjugated Polymer Nanoparticle Fluorescence. *Chem. Commun.* **2016**, *52*, 4144−4147.
(22) Davis, C. M.; Childress, E. S.; Harbron, E. J. Ensemble and Single-Particle Fluorescence Photomodulation in Diarylethene-Doped Conjugated Polymer Nanoparticles. *J. Phys. Chem. C* **2011**, *115*, 19065−19073.
(23) Harbron, E. J.; Davis, C. M.; Campbell, J. K.; Allred, R. M.; Kovary, M. T.; Economou, N. J. Photochromic Dye-Doped Conjugated Polymer Nanoparticles: Photomodulated Emission and Nanoenvironmental Characterization. *J. Phys. Chem. C* **2009**, *113*, 13707−13714.
(24) Kuo, C.-T.; Thompson, A. M.; Gallina, M. E.; Ye, F.; Johnson, E. S.; Sun, W.; Zhao, M.; Yu, J.; Wu, I.-C.; Fujimoto, B.; et al. Optical Painting and Fluorescence Activated Sorting of Single Adherent Cells Labelled with Photoswitchable Pdots. *Nat. Commun.* **2016**, *7*, 11468.
(25) Osakada, Y.; Fukaminato, T.; Ichinose, Y.; Fujitsuka, M.; Harada, Y.; Majima, T. Live Cell Imaging Using Photoswitchable Diarylethene-Doped Fluorescent Polymer Dots. *Chem.—Asian J.* **2017**, *12*, 2660−2665.
(26) Osakada, Y.; Hanson, L.; Cui, B. Diarylethene Doped Biocompatible Polymer Dots for Fluorescence Switching. *Chem. Commun.* **2012**, *48*, 3285−3287.
(27) Jeong, K.; Park, S.; Lee, Y.-D.; Lim, C.-K.; Kim, J.; Chung, B. H.; Kwon, I. C.; Park, C. R.; Kim, S. Conjugated Polymer/Photochromophore Binary Nanococktails: Bistable Photoswitching of Near-Infrared Fluorescence for In Vivo Imaging. *Adv. Mater.* **2013**, *25*, 5574−5580.
(28) Watanabe, K.; Hayasaka, H.; Miyashita, T.; Ueda, K.; Akagi, K. Dynamic Control of Full-Colored Emission and Quenching of Photoresponsive Conjugated Polymers by Photostimuli. *Adv. Funct. Mater.* **2015**, *25*, 2794−2806.
(29) Feng, G.; Ding, D.; Li, K.; Liu, J.; Liu, B. Reversible Photoswitching Conjugated Polymer Nanoparticles for Cell and Ex Vivo Tumor Imaging. *Nanoscale* **2014**, *6*, 4141−4147.
(30) Chan, Y.-H.; Gallina, M. E.; Zhang, X.; Wu, I.-C.; Jin, Y.; Sun, W.; Chiu, D. T. Reversible Photoswitching of Spiropyran-Conjugated Semiconducting Polymer Dots. *Anal. Chem.* **2012**, *84*, 9431−9438.
(31) Chen, J.; Wang, D.; Turshatov, A.; Muñoz-Espí, R.; Ziener, U.; Koynov, K.; Landfester, K. One-Pot Fabrication of Amphiphilic Photoswitchable Thiophene-Based Fluorescent Polymer Dots. *Polym. Chem.* **2013**, *4*, 773−781.
(32) Anwar, N.; Willms, T.; Grimme, B.; Kuehne, A. J. C. Light-Switchable and Monodisperse Conjugated Polymer Particles. *ACS Macro Lett.* **2013**, *2*, 766−769.
(33) Liu, R.; Yang, Y.; Cui, Q.; Xu, W.; Peng, R.; Li, L. A Diarylethene-Based Photoswitch and Its Photomodulation of the Fluorescence of Conjugated Polymers. *Chem.—Eur. J.* **2018**, *24*, 17756−17766.
(34) Jana, B.; Bhattacharyya, S.; Patra, A. Perspective of Dye-Encapsulated Conjugated Polymer Nanoparticles for Potential Applications. *Bull. Mater. Sci.* **2018**, *41*, 122.
(35) Zhang, X.; Kurimoto, A.; Frank, N. L.; Harbron, E. J. Controlling Photoswitching via pcFRET in Conjugated Polymer Nanoparticles. *J. Phys. Chem. C* **2018**, *122*, 22728−22737.
(36) Ortiz, A. M. O.; George, O.; Jasim, K.; Gesquiere, A. J. Photodynamic Therapy with Conjugated Polymer Nanoparticles: Recent Advances and Therapeutic Considerations. *J. Cancer Treat. Diagn.* **2018**, *2*, 1−6.
(37) Ibarra, L. E.; Porcal, G. V.; Macor, L. P.; Ponzio, R. A.; Spada, R. M.; Lorente, C.; Chesta, C. A.; Rivarola, V. A.; Palacios, R. E. Metallated Porphyrin-Doped Conjugated Polymer Nanoparticles for Efficient Photodynamic Therapy of Brain and Colorectal Tumor Cells. *Nanomedicine* **2018**, *13*, 605−624.
(38) Spada, R. M.; Macor, L. P.; Hernández, L. I.; Ponzio, R. A.; Ibarra, L. E.; Lorente, C.; Chesta, C. A.; Palacios, R. E. Amplified Singlet Oxygen Generation in Metallated-Porphyrin Doped Conjugated Polymer Nanoparticles. *Dyes Pigm.* **2018**, *149*, 212−223.
(39) Haupt, S.; Lazar, I.; Weitman, H.; Shav-Tal, Y.; Ehrenberg, B. FRET Energy Transfer via Pdots Improves the Efficiency of Photodynamic Therapy and Leads to Rapid Cell Death. *J. Photochem. Photobiol., B* **2016**, *164*, 123−131.
(40) Li, S.; Chang, K.; Sun, K.; Tang, Y.; Cui, N.; Wang, Y.; Qin, W.; Xu, H.; Wu, C. Amplified Singlet Oxygen Generation in Semiconductor Polymer Dots for Photodynamic Cancer Therapy. *ACS Appl. Mater. Interfaces* **2016**, *8*, 3624−3634.
(41) Irie, M. Discovery and Development of Photochromic Diarylethenes. *Pure Appl. Chem.* **2015**, *87*, 617−626.
(42) Irie, M.; Fukaminato, T.; Matsuda, K.; Kobatake, S. Photochromism of Diarylethene Molecules and Crystals: Memories, Switches, and Actuators. *Chem. Rev.* **2014**, *114*, 12174−12277.
(43) Irie, M.; Sakemura, K.; Okinaka, M.; Uchida, K. Photochromism of Dithienylethenes with Electron-Donating Substituents. *J. Org. Chem.* **1995**, *60*, 8305−8309.
(44) Lin, Y.; Dong, C.; Cao, F.; Xiong, L.; Gu, H.; Xu, H. Size-Dependent Optical Properties of Conjugated Polymer Nanoparticles. *RSC Adv.* **2017**, *7*, 55957−55965.
(45) Liu, Z.; Sun, Z.; Di, W.; Qin, W.; Yuan, Z.; Wu, C. Brightness Calibrates Particle Size in Single Particle Fluorescence Imaging. *Opt. Lett.* **2015**, *40*, 1242−1245.
(46) Wu, P.-J.; Kuo, S.-Y.; Huang, Y.-C.; Chen, C.-P.; Chan, Y.-H. Polydiacetylene-Enclosed Near-Infrared Fluorescent Semiconducting Polymer Dots for Bioimaging and Sensing. *Anal. Chem.* **2014**, *86*, 4831−4839.
(47) Montalti, M.; Credi, A.; Prodi, L.; Gandolfi, M. T. Chemical Actinometry. *Handbook of Photochemistry*; CRC Press, 2006; pp 601−616.
(48) Glaze, A. P.; Heller, H. G.; Whittall, J. Photochromic Heterocyclic Fulgides. Part 7. (E)-Adamantylidene-[I -(2,5- Dimethyl-3-Furyl)Ethyl Idenelsuccinic Anhydride and Derivatives: Model Photochromic Compounds for Optical Recording Media. *J. Chem. Soc., Perkin Trans. 2* **1992**, 591−594.
(49) Gehlen, M. H. The Centenary of the Stern-Volmer Equation of Fluorescence Quenching: From the Single Line Plot to the SV Quenching Map. *J. Photochem. Photobiol., C* **2020**, *42*, 100338.
(50) Kwon, D.-H.; Shin, H.-W.; Kim, E.; Boo, D. W.; Kim, Y.-R. Photochromism of Diarylethene Derivatives in Rigid Polymer Matrix: Structural Dependence, Matrix Effect, and Kinetics. *Chem. Phys. Lett.* **2000**, *328*, 234−243.

https://dx.doi.org/10.1021/acs.jpcc.0c09084
J. Phys. Chem. C 2020, 124, 26474−26485

(51) Wu, C.; McNeill, J. Swelling-Controlled Polymer Phase and Fluorescence Properties of Polyfluorene Nanoparticles. *Langmuir* **2008**, *24*, 5855−5861.
(52) Xie, R.; Weisen, A. R.; Lee, Y.; Aplan, M. A.; Fenton, A. M.; Masucci, A. E.; Kempe, F.; Sommer, M.; Pester, C. W.; Colby, R. H.; Gomez, E. D. Glass Transition Temperature from the Chemical Structure of Conjugated Polymers. *Nat. Commun.* **2020**, *11*, 893.
(53) Thomas, S. W.; Joly, G. D.; Swager, T. M. Chemical Sensors Based on Amplifying Fluorescent Conjugated Polymers. *Chem. Rev.* **2007**, *107*, 1339−1386.
(54) Liu, Y.; Ogawa, K.; Schanze, K. S. Conjugated Polyelectrolytes as Fluorescent Sensors. *J. Photochem. Photobiol., C* **2009**, *10*, 173−190.
(55) Wu, C.; Peng, H.; Jiang, Y.; McNeill, J. Energy Transfer Mediated Fluorescence from Blended Conjugated Polymer Nanoparticles. *J. Phys. Chem. B* **2006**, *110*, 14148−14154.
(56) Wang, X.; Groff, L. C.; McNeill, J. D. Multiple Energy Transfer Dynamics in Blended Conjugated Polymer Nanoparticles. *J. Phys. Chem. C* **2014**, *118*, 25731−25739.
(57) Lakowicz, J. R. *Principles of Fluorescence Spectroscopy*, 3rd ed.; Kluwer Academic/Plenum: New York, 2006.
(58) Díaz, S. A.; Gillanders, F.; Jares-Erijman, E. A.; Jovin, T. M. Photoswitchable Semiconductor Nanocrystals with Self-Regulating Photochromic Forster Resonance Energy Transfer Acceptors. *Nat. Commun.* **2015**, *6*, 6036.
(59) Mekler, V. M.; Averbakh, A. Z.; Sudarikov, A. B.; Kharitonova, O. V. Fluorescence Energy Transfer-Sensitized Photobleaching of a Fluorescent Label as a Tool to Study Donor-Acceptor Distance Distributions and Dynamics in Protein Assemblies: Studies of a Complex of Biotinylated IgM with Streptavidin and Aggregates of Concanavalin A. *J. Photochem. Photobiol., B* **1997**, *40*, 278−287.
(60) Herder, M.; Schmidt, B. M.; Grubert, L.; Pätzel, M.; Schwarz, J.; Hecht, S. Improving the Fatigue Resistance of Diarylethene Switches. *J. Am. Chem. Soc.* **2015**, *137*, 2738−2747.
(61) Warford, C. C.; Carling, C.-J.; Branda, N. R. From Slow to Fast-the User Controls the Rate of the Release of Molecules from Masked Forms Using a Photoswitch and Different Types of Light. *Chem. Commun.* **2015**, *51*, 7039−7042.
(62) Williams, D. E.; Martin, C. R.; Dolgopolova, E. A.; Swifton, A.; Godfrey, D. C.; Ejegbavwo, O. A.; Pellechia, P. J.; Smith, M. D.; Shustova, N. B. Flipping the Switch: Fast Photoisomerization in a Confined Environment. *J. Am. Chem. Soc.* **2018**, *140*, 7611−7622.
(63) Walton, I. M.; Cox, J. M.; Benson, C. A.; Patel, D. G.; Chen, Y.-S.; Benedict, J. B. The Role of Atropisomers on the Photo-Reactivity and Fatigue of Diarylethene-Based Metal-Organic Frameworks. *New J. Chem.* **2016**, *40*, 101−106.
(64) Deniel, M. H.; Lavabre, D.; Micheau, J.-C. In *Organic Photochromic and Thermochromic Compounds*; Crano, J. C., Guglielmetti, R. J., Eds.; Kluwer Academic: New York, 1999; pp 167−209.
(65) Delbaere, S.; Vermeersch, G.; Micheau, J.-C. Quantitative Analysis of the Dynamic Behaviour of Photochromic Systems. *J. Photochem. Photobiol., C* **2011**, *12*, 74−105.
(66) Sumi, T.; Takagi, Y.; Yagi, A.; Morimoto, M.; Irie, M. Photoirradiation Wavelength Dependence of Cycloreversion Quantum Yields of Diarylethenes. *Chem. Commun.* **2014**, *50*, 3928−3930.
(67) Ishibashi, Y.; Umesato, T.; Fujiwara, M.; Une, K.; Yoneda, Y.; Sotome, H.; Katayama, T.; Kobatake, S.; Asahi, T.; Irie, M.; Miyasaka, H. Solvent Polarity Dependence of Photochromic Reactions of a Diarylethene Derivative As Revealed by Steady-State and Transient Spectroscopies. *J. Phys. Chem. C* **2016**, *120*, 1170−1177.
(68) Miller, R. A.; Presley, A. D.; Francis, M. B. Self-Assembling Light-Harvesting Systems from Synthetically Modified Tobacco Mosaic Virus Coat Proteins. *J. Am. Chem. Soc.* **2007**, *129*, 3104−3109.
(69) Jana, B.; Ghosh, A.; Patra, A. Photon Harvesting in Conjugated Polymer-Based Functional Nanoparticles. *J. Phys. Chem. Lett.* **2017**, *8*, 4608−4620.
(70) Jeong, J.-E.; Uddin, M. A.; Ryu, H. S.; Kim, H.-C.; Kang, M.; Joung, J. F.; Park, S.; Shim, S.-H.; Woo, H. Y. Green-, Red-, and Near-Infrared-Emitting Polymer Dot Probes for Simultaneous Multicolor Cell Imaging with a Single Excitation Wavelength. *Chem. Mater.* **2020**, *32*, 6685−6696.
(71) Sun, F.; Zhang, F.; Zhao, F.; Zhou, X.; Pu, S. Preparation and Photochromic Properties of Diarylethene Nanoparticles. *Chem. Phys. Lett.* **2003**, *380*, 206−212.

https://dx.doi.org/10.1021/acs.jpcc.0c09084
J. Phys. Chem. C 2020, 124, 26474−26485